arXiv:1204.2419v2 [cond-mat.mtrl-sci] 3 Jul 2012

On the large magnetic anisotropy of Fe_2P

M. Costa,[1,2] O. Gråsäs,[2] A. Bergman,[2] P. Venezuela,[1] P. Nordblad,[3] M. Klintenberg,[2] and O. Eriksson[2]

[1] *Instituto de Fisica, Universidade Federal Fluminense, 24210-346 Niterói, Rio de Janeiro, Brazil*
[2] *Department of Physics and Astronomy, Uppsala University, Box 516, 75121 Uppsala, Sweden*
[3] *Department of Engineering Science, Uppsala University,Box 534, 75121, Uppsala, Sweden*

We present an investigation on the large magnetic anisotropy of Fe_2P, based on *Ab Initio* density-functional theory calculations, with a full potential linear muffin-tin orbital (FP-LMTO) basis. We obtain an uniaxial magnetic anisotropy energy (MAE) of 664 μeV/f.u., which is in decent agreement with experimental observations. Based on a band structure analysis the microscopical origin of the large magnetic anisotropy is explained. We also show that by straining the crystal structure, the MAE can be enhanced further.

INTRODUCTION

Magnetic materials with large magnetic anisotropy (MAE) have been used in many applications. Until recently the dominating class of materials used for such applications, apart from hard ferrites, were rare-earth based magnets, e.g. $Nd_2Fe_{14}B$ [1], in which the large magnetic anisotropy energy is provided by the rare-earth atoms, and the large saturation moment (M_s) at finite temperature is due to the Fe atoms. It has however been pointed out that other permanent magnets should be investigated, from an application point of view, since a general access to rare-earth elements is far from guaranteed [2]. Among such materials the iron-phosphide Fe_2P stands out as a particularly interesting material, due its known large MAE and sufficient large value of saturation moment . In addition Fe_2P is composed of cheap and widely available elements.

Transition metal pnictides and chalcogenides are not the only large MAE materials that have been investigated so far. For instance, a large saturation moment was suggested in a nano-laminate of a 3d metal (Fe) and a rare earth metal (Gd) in Ref.3. Also, a large magnetic anisotropy in FePt was verified experimentally as well as from first principles theory [4–8]. Furthermore, the predicted large MAE of a tetragonally strained FeCo-alloy [9] was verified experimentally [10].

In this report we focus on the MAE of Fe_2P, since it is large and hitherto unexplained. In order to find a microscopic description of the large MAE of this compound we have performed first principles calculations, using a relativistic formulation of the Kohn-Sham equation. There are several experimental studies concerning the ordering temperature, MAE, saturation moment, hyperfine field and isomer-shift of Fe_2P [11–14]. In addition, a theoretical analysis was made earlier by Wohlfarth [15, 16], and a subsequent theoretical work addressed the magnetism of Fe_2P using electronic structure calculations [17, 18]. An excellent overview of the magnetic properties of Fe_2P and similar transition metal pnictides and chalcogenides can be found in Ref.19.

In its crystal structure Fe_2P (Hexagonal C_{22} with space group $P\bar{6}2m$, No. 189) [20, 21] has two Fe sites. The Fe-I site has a magnetic moment close to 1 μ_B/atom, and the Fe-II site has a magnetic moment close to 2 μ_B/atom (In Fig. 1 the structure of Fe_2P is shown). The material has an observed MAE of 500 μeV/f.u. [19], with the crystallographic c-axis being the magnetization easy axis. The microscopic mechanism for this large MAE is however unknown. It is the motivation of the present study to find this mechanism, and to suggest Fe_2P based alloys with enhanced values of MAE.

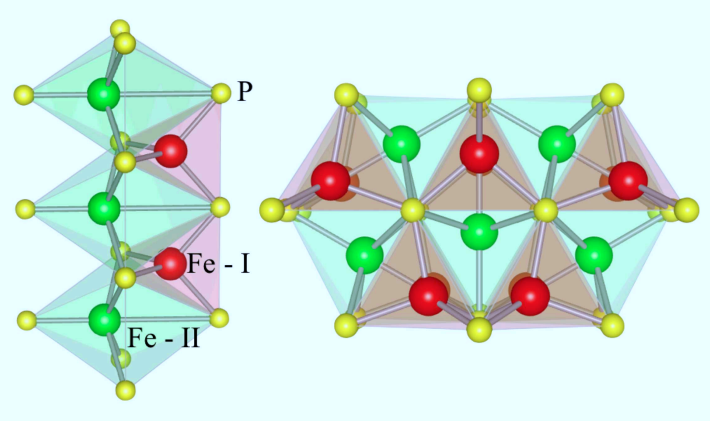

Fig. 1: (color online) Fe_2P crystal structure. Fe-I tetrahedral-sites (red), Fe-II pyramidal-sites (green) and P atoms (yellow).

COMPUTATIONAL DETAILS

We used a full potential linear muffin-tin (FP-LMTO) method [22], with a relativistic formulation, where the spin-orbit coupling is included inside the muffin-tins spheres, at the variational step. The muffin-tins are centered on atomic sites, and a combination of radial functions multiplied by spherical harmonics are used to expand the electronic density and potential inside each muffin-tin. In the interstitial region a combination of Hankel and Neumann functions are used as basis functions. We calculated the MAE by the magnetic force the-

orem [23]. A scalar relativistic calculation, with common symmetry of both magnetization directions, is first performed to obtain a self-consistent potential. With this potential fixed one performs a fully-relativistic calculation for each magnetization orientations ($\hat{n}_i$). The E_{MAE} (magnetic anisotropy energy) is then calculated from the expression

$$E_{MAE} = \sum_{i,k}^{occ.} e_i(\hat{n}_2, k) - \sum_{i,k}^{occ.} e_i(\hat{n}_1, k). \quad (1)$$

Here $e_i(\hat{n}, k)$ is the Kohn-Sham eigenvalues evaluated for each magnetization orientation. In Eq.1, i labels the occupied states and k the **k**-points in the Brillouin zone, whereas $\hat{n}_1 = 0001$ (c-axis) and $\hat{n}_2 = 1000$.

The modified tetrahedron method (MTM) [24] was used for integration in the Brillouin zone (BZ), 36002 **k**-points were used (for a calculation with 50626 **k**-points the MAE deviates only 0.1 %), in irreducible part of BZ, to guarantee the convergence.

RESULTS

Our main result is shown in Fig. 2, where we display the calculated MAE as a function of the strain. Note that we have used the room temperature lattice constant as reference level, having room temperature applications in mind. It is clear from the figure that theory reproduces the observed easy axis (0001) and that the calculated MAE is of the same order of magnitude as the experimental one. The theory overestimates the value of the MAE by 32 %, when a comparison is made between the experimental low temperature value (red square, taken at 4 K) and the lattice parameters corresponding to this temperature (which in Fig.2 corresponds to a - 0.55 %). The strain state of the low temperature lattice constant is calculated from the work of Fujii *et. al.* [12] who reported measurements for the thermal expansion of the Fe_2P in the temperature range of 60 to 550 K. Using this thermal expansion data the 4 K lattice parameters were estimated. The agreement between calculated and measured MAE obtained here is typical, when compared to other calculations [5, 6, 25], and primarily reflects the extremely delicate nature of the MAE in general. A very important result shown in Fig. 2, however, is that with an applied strain to the lattice it is possible to influence the MAE quite substantially. In these calculations, we applied strain, keeping a constant volume. Increasing the c value by 1% affects the MAE to be enhanced by ~ 15 %, which is the maximum value of the calculated MAE. For strain values higher than 1%, Fig. 2 shows that the MAE decreases almost linearly. Reducing the c-axis is not favorable for the MAE, here we note a monotonically decreasing trend, with a minimum observed at -8%. Unfortunately most dopings on the P site, e.g. with Si or B, results in a reduced c/a ratio [12, 20, 26].

The magnetic moment of Fe_2P changes much less with strain when compared to the MAE, as the inset of Fig. 2 shows. At 1% strain the calculated moment is 3.03 μ_B/f.u., which is -0.4 % of the zero strained system. The magnetic moment increases however slightly for negative values of strain. Overall our calculated moments agree well with the observed number of 2.94 μ_B/f.u [12].

The Fig. 2 shows data for a volume conserving strain (except the red square which corresponds to a volume which is minutely smaller than the volume used for the other data points). For comparison we also show in Fig. 3 the MAE as function of strain in two non-volume conserving regimes.

This involves strain of the c-axis while a and b are fixed as well as strain of the ab-axis while c axis is fixed. For c-axis (ab-axis) strain a maximum MAE value of 800 μeV (807 μeV) is obtained for 2% (-1%) strain. Experimental doping on the P site with B results in a reduced c/a axis (negative strain) and a reduced volume [12, 20, 26], in this case a predicted MAE with doping is best evaluated by inspection of the non-volume conserving curve in Fig. 3. Doping with Si keeps the volume essentially constant while reducing the c/a ratio, and for this doping element the predicted MAE is best evaluated from the volume conserving curve, which shows a decreased MAE. The MAE was actually calculated using the structural cell parameters for 10 % Si doping [19], and 593 μeV MAE was obtained, showing the expected reduction. For 10% Si doping the experimental Curie temperature (T_c) is 370 K (an increase of 70 % when compared with the undoped case), which is promising for stabilizing a material which at room temperature has a large MAE. Further investigations are necessary to consider the chemical effect impact on the MAE.

Both these predicted changes of the MAE with doping rely on the applicability of the rigid band approximation. They have not been evaluated experimentally, and a verification or refutal of this prediction would be interesting.

The strong variation of the MAE with strain in Fig. 2 is interesting and requires further analysis. On a simple model level, the uniaxial MAE can be treated in second-order perturbation theory, and computed as the difference of the second order correction to the energy ($E_q^{ss'}[\hat{n}]$) between two magnetization directions as in Eq. 2, with a sum over the sites q, over occupied (s) and unoccupied (s') spin characters, respectively; [27]

$$\Delta E_{SO} = \sum_{qss'} \Delta E_q^{ss'} = \sum_{qss'} \{E_q^{ss'}(\hat{n}_2) - E_q^{ss'}(\hat{n}_1)\}, \quad (2)$$

where the energy correction is given by,

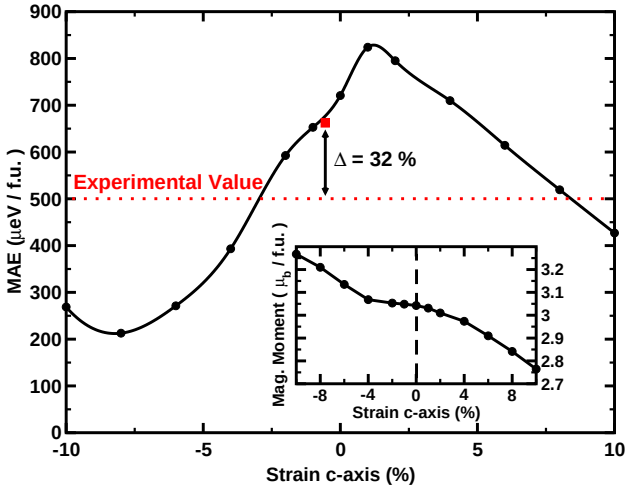

Fig. 2: (color online) Calculated MAE as function of the strain. Positive values of the strain correspond to an increased c/a ratio (at constant volume). Positive values of the MAE correspond to the c-axis being the easy axis. The inset shows the calculated magnetic moment as a function of strain. The square (red) is the MAE value for the estimated 4 K lattice parameters.

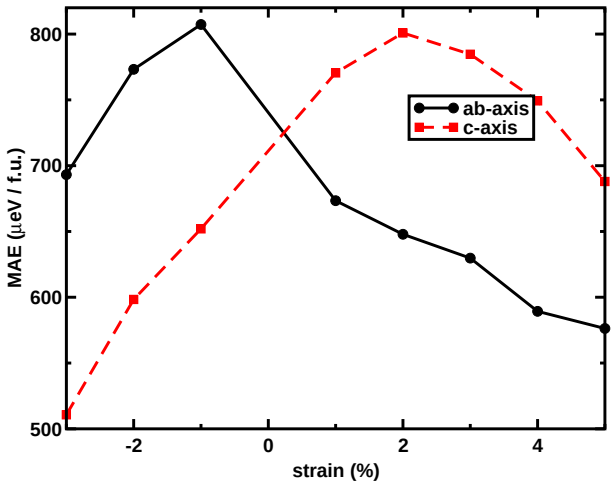

Fig. 3: (color online) Calculated MAE as function of the strain of the c-axis with a and b fixed (red squares) and strain on the ab-axis with c fixed (black circles).

$$E_q^{ss'}(\hat{n}) = -\sum_{\mathbf{k}ij}\sum_{q'}\sum_{\{m\}} n_{\mathbf{k}is,qm,q'm'} n_{\mathbf{k}js',q'm'',qm'''} \times \frac{\langle qms|\hat{H}_{SO}(\hat{n})|qm'''s'\rangle\langle q'm''s'|\hat{H}_{SO}(\hat{n})|q'm's\rangle}{\epsilon_{\mathbf{k}j} - \epsilon_{\mathbf{k}i}}. \quad (3)$$

In Eq. 3 there is a sum over **k** points in the Brillouin zone, i and j label the occupied and unoccupied states, s and s' run over the spin character of the states and m, m′, m″, m‴ run over the magnetic quantum numbers. The basis functions $|qlms\rangle$ are characterized by the site q, azimuthal (l), magnetic (m) and spin (s) quantum numbers and $\epsilon_{\mathbf{k}i}$ ($\epsilon_{\mathbf{k}j}$) are the electronic eigenvalues for the occupied (unoccupied) states. The hybridization is considered in the band character $n_{\mathbf{k}is,qm,q'm'}$, which allows mixing of basis functions on different sites.

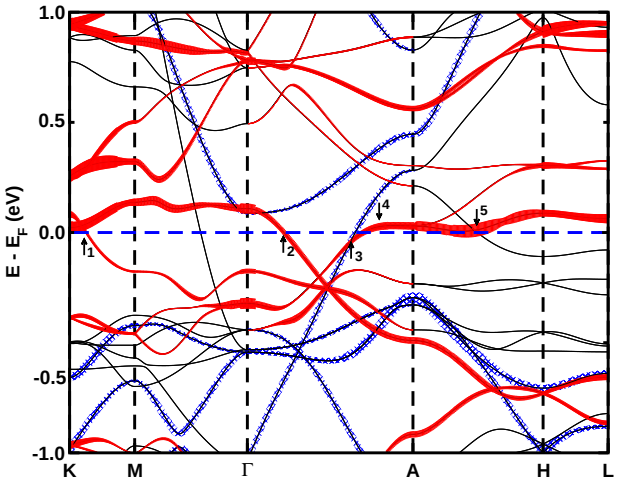

Fig. 4: (color online) Band structure of Fe_2P calculated without spin-orbit coupling (the band thickness represents the weight of Fe-II, l=2 and m=-2 state). Red (solid) is the spin up character and blue (striped) is the spin down. The Fermi level (E_F) is placed at E=0.

Since the electronic eigenvalues ($\epsilon_{\mathbf{k}i}$) appear in Eq. 3, it is relevant to inspect the band structure along the high symmetry lines of the hexagonal lattice. Hence, we show the calculated energy bands in Fig. 4, where the thickness of the bands represents the weight of the Fe-II, l=2 and m=-2 state. The bands that contribute the most to the MAE are highlighted by the arrows 1 to 5. At $\frac{1}{4}$(K-M), arrow 1, the occupied and unoccupied bands have mainly character from l=2 and m=±2 quantum numbers, and these bands interact through the $l_z s_z$ term of the spin-orbit coupling (SOC) Hamiltonian, resulting in a large negative contribution. A similar mechanism is observed at $\frac{3}{4}$(Γ-A), arrow 4. This is illustrated further using a calculation with spin-orbit coupling included, in Fig. 5 a), in a region zoomed in around the Fermi level, see the highlighted areas. One can see the splitting of the bands when the spin quantization axis is along the 0001 crystallographic direction. The splitting of these bands is not observed for the 100 axis, as observed in Fig. 5 b). At arrows 2, 3 and 5 the occupied and unoccupied bands have different m quantum numbers, m=±2 and m=0 (m=±1) for the occupied (unoccupied) bands, the SOC interaction via the terms : $l_+ s_- + l_- s_+$, give large positive contributions. As a general rule if the occupied and unoccupied bands have the same (different) m quantum number, the magnetization is favored to lie along

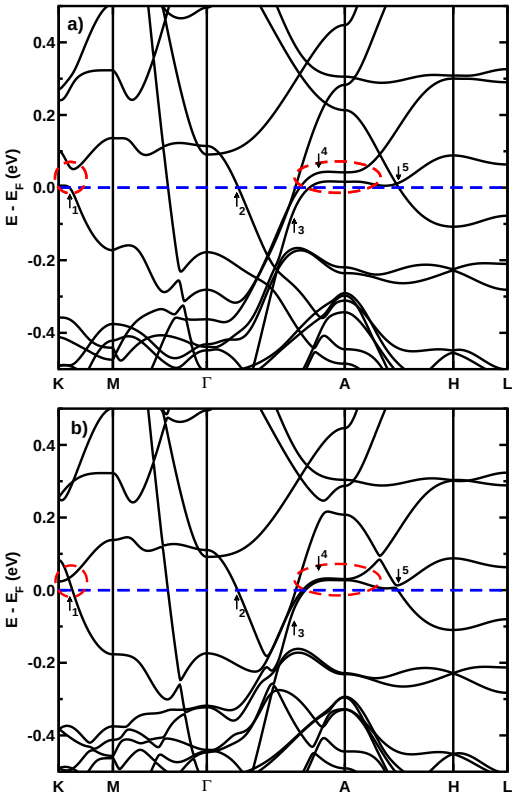

Fig. 5: (color online) Zero strain band structure of Fe_2P calculated with spin-orbit coupling, magnetization along the a) 001 and b) 100 crystallographic axis. The Fermi level (E_F) is placed at E=0.

the 001 (100) axis [28].

To understand the enhancement of the MAE under uniaxial strain, the bandstructure was calculated for the 1 % volume conserving strain (Fig 6 a). The overall bandstructure is not changed, due to the strain, only a rigid shift is observed. Without SOC the flat bands around the A point lies on the Fermi level. As pointed out before these bands are split due to SOC for a magnetization along the 001 axis. One of the bands become fully occupied and the other fully unoccupied, given that these bands are very close in energy a large contribution to the MAE is expected. Indeed this is confirmed in Fig 6 b) (upper panel) where the MAE for each **k**-point ($E_{MAE}[\mathbf{k}]$) along the high symmetry lines of the hexagonal cell is showed, for the zero and 1% (volume conserving) strained system. For the zero strain one can see a sharp negative peak for the MAE (negative values favors the 001 axis) around arrows 1 and 4. For 1% strain the peak at arrow 4 gets broadened explaining the increasing of the MAE.

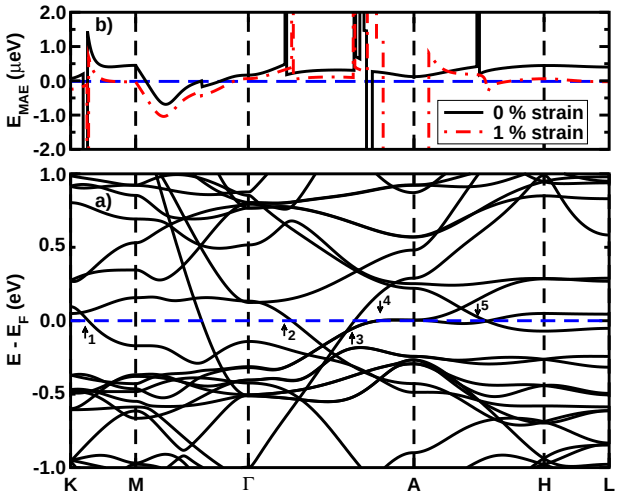

Fig. 6: (color online) a) Band structure of Fe_2P calculated with 1 % of strain on the c-axis and b) MAE along the high symmetry directions. The Fermi Level (E_F) is placed at E=0.

CONCLUSION

In conclusion we have studied the uniaxial MAE of Fe_2P by *Ab Initio* calculations. Our theory reproduces the observed 0001-easy axis with a MAE of 664 μeV/f.u. This should be compared to an experimental value of $\sim$ 500 μeV/f.u.(2.32 MJ/m^3) This is an acceptable agreement between theory and experiment, when having in mind the extremely delicate nature of the MAE and the typical low energy differences associated with it. The size of the MAE of Fe_2P should be compared to other hard magnetic materials like FePt 1.2 meV/f.u. (6.6 MJ/m^3) [4] and $Nd_2Fe_{12}B$ 6.7 meV/f.u. (4.9 MJ/m^3) [29]. As to the magnetic moments our calculations give value of 3.04 μ_B/f.u., which agrees well with the experimental moment of 2.94 μ_B/f.u.

We have analyzed the origin of the MAE by a detailed band and **k**-point resolved property, and show that the positions of the different energy bands around the Fermi level critically determine that MAE. Since these bands can be moved up or down in energy with an applied strain, it seems that this is an important avenue with which to influence the MAE of Fe_2P and Fe_2P-based alloys. Consequently we find from our MAE calculations that it is possible to influence the MAE quite strongly with an applied strain, both in a volume conserving and a non-volume conserving mode. This opens up possibilities to use Fe_2P and alloys of this material, as a platform for searching for new permanent magnetic materials that don't contain rare-earth elements.

Support by the Swedish Research Council (VR) is acknowledged, as is the the European Research Council (project 247062 - ASD), the KAW foundation, eSSENCE, STEM, STANDUPP, EU project REFREEMAG and the

Swedish National Infrastructure for Computing (SNIC). Valuable discussions with Laszlo Szunyogh are acknowledged.

[1] J. M. D. Coey, editor. *Rare-Earth Iron Permanent Magnets*. Oxford University Press, 1996.

[2] David Kramer. Concern grows over China's dominance of rare-earth metals. *Phys. Today*, 63(5):22, 2010.

[3] Biplab Sanyal, Carolin Antoniak, Till Burkert, Bernhard Krumme, Anne Warland, Frank Stromberg, Christian Praetorius, Kai Fauth, Heiko Wende, and Olle Eriksson. Forcing Ferromagnetic Coupling Between Rare-Earth-Metal and 3d Ferromagnetic Films. *Phys. Rev. Lett.*, 104(15), April 2010.

[4] Shouheng Sun, C. B. Murray, Dieter Weller, Liesl Folks, and Andreas Moser. Monodisperse fept nanoparticles and ferromagnetic fept nanocrystal superlattices. *Science*, 287(5460):1989–1992, 2000. doi: 10.1126/science.287.5460.1989. URL `http://www.sciencemag.org/content/287/5460/1989.abstract`.

[5] Gho Daalderop, PJ Kelly, and MFH Schuurmans. Magnetocrystalline Anisotropy and Orbital Moments in Transition-Metal Compounds. *Phys. Rev. B*, 44(21): 12054–12057, 1991.

[6] Till Burkert, Olle Eriksson, Sergei Simak, Andrei Ruban, Biplab Sanyal, Lars Nordström, and John Wills. Magnetic anisotropy of L10 FePt and Fe(1-x)Mn(x)Pt. *Phys. Rev. B*, 71(13), April 2005.

[7] J B Staunton, S Ostanin, S S A Razee, B Gyorffy, L Szunyogh, B Ginatempo, and Ezio Bruno. Long-range chemical order effects upon the magnetic anisotropy of FePt alloys from an ab initioelectronic structure theory. *J. Phys.: Condens. Matter*, 16(48):S5623–S5631, November 2004.

[8] Sumanta Bhandary, Oscar Grånäs, Laszlo Szunyogh, Biplab Sanyal, Lars Nordström, and Olle Eriksson. Route towards finding large magnetic anisotropy in nanocomposites: Application to a W_(1-x)Re_(x)/Fe multilayer. *Phys. Rev. B*, 84(9), September 2011.

[9] Till Burkert, Lars Nordström, Olle Eriksson, and Olle Heinonen. Giant Magnetic Anisotropy in Tetragonal FeCo Alloys. *Phys. Rev. Lett.*, 93(2), July 2004.

[10] Gabriella Andersson, Till Burkert, Peter Warnicke, Matts Björck, Biplab Sanyal, Cyril Chacon, Claudia Zlotea, Lars Nordström, Per Nordblad, and Olle Eriksson. Perpendicular Magnetocrystalline Anisotropy in Tetragonally Distorted Fe-Co Alloys. *Phys. Rev. Lett.*, 96(3), January 2006.

[11] R Wappling, L Häggström, T Ericsson, S Devanarayanan, E Karlsson, B Carlsson, and S. Rundqvist. First-Order Magnetic Transition, Magnetic-Structure, and Vacancy Distribution in Fe2p. *J Solid State Chem*, 13(3):258–271, 1975.

[12] H Fujji, T Hokabe, T Kamigaichi, and T Okamoto. Magnetic-Properties of Fe2p Single-Crystal. *J. Phys. Soc. Jpn.*, 43(1):41–46, 1977.

[13] R Chandra, S Bjarman, and T ERICSSON. ScienceDirect.com - Journal of Solid State Chemistry - A Mössbauer and X-ray study of Fe2P(1-x)B(x) compounds (x ¡ 0.15). *Journal of Solid State . . .*, 1980.

[14] O Eriksson and A Svane. Isomer shifts and hyperfine fields in iron compounds. *J. Phys.: Condens. Matter*, 1: 1589, 1989.

[15] E P Wohlfarth. First and second order transitions in some metallic ferromagnets. *J. Appl. Phys.*, 50(B11): 7542, 1979.

[16] T. Moriya and K. Usami. Coexistence of ferro-and antiferromagnetism and phase transitions in itinerant electron systems. *Solid State Communications*, 23(12):935–938, 1977.

[17] S Ishida, S Asano, and J Ishida. Electronic-Structures and Magnetic-Properties of Mn2p, Fe2p, Ni2p. *J Phys F Met Phys*, 17(2):475–482, 1987.

[18] O Eriksson, J Sjöström, B Johansson, L Häggström, and HL Skriver. Itinerant ferromagnetism in Fe2P. *J Magn Magn Mater*, 74(3):347–358, 1988.

[19] K.H.J. Buschow, editor. volume 6 of *Handbook of Magnetic Materials*. Elsevier, 1991. doi: 10.1016/S1567-2719(05)80052-6. URL `http://www.sciencedirect.com/science/article/pii/S156727190`

[20] Bertil Carlsson, Margareta Gölin, and Stig Rundqvist. Determination of the homogeneity range and refinement of the crystal structure of Fe2P. *J Solid State Chem*, 8 (1):57–67, September 1973.

[21] C Ortiz, O Eriksson, and M Klintenberg. Data mining and accelerated electronic structure theory as a tool in the search for new functional materials. *Computational Materials Science*, 44(4):1042–1049, February 2009.

[22] J M Wills, M Alouani, P Andersson, A Delin, O Eriksson, and A Grechnev. *Full-Potential Electronic Structure Method, Energy and Force Calculations with Density Functional and Dynamical Mean Field Theory*. Springer Series in Solid-State Sciences. Springer, Berlin ; Heidelberg ; New York, 2010.

[23] HJF Jansen. Magnetic anisotropy in density-functional theory. *Phys. Rev. B*, 59(7):4699–4707, 1999.

[24] PE Blöchl, O Jepsen, and OK Andersen. Improved Tetrahedron Method for Brillouin-Zone Integrations. *Phys. Rev. B*, 49(23):16223–16233, 1994.

[25] J Trygg, B Johansson, O Eriksson, and JM Wills. Total-Energy Calculation of the Magnetocrystalline Anisotropy Energy in the Ferromagnetic 3d Metals. *Phys. Rev. Lett.*, 75(15):2871–2874, 1995.

[26] Hironobu Fujii, Shigehiro Komura, Takayoshi Takeda, Tetsuhiko Okamoto, Yuji Ito, and Jun Akimitsu. Polarized neutron diffraction study of fe_2p single crystal. *Journal of the Physical Society of Japan*, 46(5): 1616–1621, 1979. doi: 10.1143/JPSJ.46.1616. URL `http://jpsj.ipap.jp/link?JPSJ/46/1616/`.

[27] C Andersson, B Sanyal, O Eriksson, L Nordström, O Karis, D Arvanitis, T Konishi, E Holub-Krappe, and J Dunn. Influence of Ligand States on the Relationship between Orbital Moment and Magnetocrystalline Anisotropy. *Phys. Rev. Lett.*, 99(17), October 2007.

[28] D Wang, R Wu, and AJ Freeman. First-principles theory of surface magnetocrystalline anisotropy and the diatomic-pair model. *Phys. Rev. B*, 47(22):14932, 1993.

[29] C Abache and J Oesterreicher. Magnetic anisotropies and spin reorientations of R2Fe14B-type compounds. *J. Appl. Phys.*, 60(10):3671, 1986.